Superoxide Radical Anion Adduct of 5,5-Dimethyl-1-pyrroline *N*-Oxide (DMPO). 2. The Thermodynamics of Decay and EPR Spectral Properties

Frederick A. Villamena,*,† John K. Merle,‡ Christopher M. Hadad,*,‡ and Jay L. Zweier*,†

Center for Biomedical EPR Spectroscopy and Imaging, The Davis Heart and Lung Research Institute, and the Division of Cardiovascular Medicine, Department of Internal Medicine, College of Medicine, and Department of Chemistry, The Ohio State University, Columbus, Ohio 43210

Received: May 10, 2005

The formation of the superoxide radical anion ($O_2^{\bullet-}$) adduct of the nitrone 5,5-dimethyl-1-pyrroline *N*-oxide (DMPO) as detected by electron paramagnetic resonance (EPR) spectroscopy is one of the most common techniques for $O_2^{\bullet-}$ detection in chemical and biological systems. However, the nature of DMPO−O_2H has confounded spin-trapping investigators over the years, since there has been no independently synthesized DMPO−O_2H to date. A density functional theory (DFT) approach was used to predict the isotropic hyperfine coupling constants arising from the N, β-H, and γ-H nuclei of DMPO−O_2H using explicit interactions with water molecules as well as via a bulk dielectric effect employing the polarizable continuum model (PCM). Theoretical calculation on the thermodynamics of DMPO−O_2H decay shows favorable intramolecular rearrangement to form a nitrosoaldehyde and a hydroxyl radical as products, consistent with experimental observations. Some pathways for the bimolecular decomposition of DMPO−O_2H and DMPO−OH have also been computed.

I. Introduction

The nitrone 5,5-dimethyl-1-pyrroline *N*-oxide (DMPO) has been the most popular spin trap used in the detection and identification of transient radicals in chemical[1−5] and biological[6−12] systems using electron paramagnetic resonance (EPR) spectroscopy. Among the reactive oxygen species (ROS), the superoxide radical anion ($O_2^{\bullet-}$) has attracted considerable attention over the past 3 decades due to the crucial role it plays (along with nitric oxide (NO)) as a modulator of cellular functions such as in cell signaling, cell proliferation, or apoptosis.[13] The ability of $O_2^{\bullet-}$ to self-dismutate to H_2O_2 producing $^{\bullet}$OH via Fenton chemistry, at high concentrations, can be detrimental to normal cellular functions.

The accurate interpretation of the DMPO−O_2H adduct spectrum has confounded most spin-trapping researchers over the years because there has been no independently synthesized DMPO−O_2H to date, and it is virtually impossible to deduce its actual form

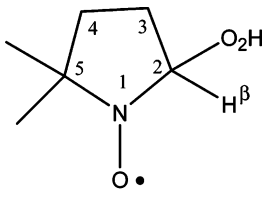

DMPO-O_2H

and property in solution due to its low concentration after spin trapping. The following questions will be investigated: Do the hyperfine coupling constants (hfcc's) arising from DMPO−O_2H adducts exclusively result from the nuclear spins of the N, β-H, and γ-H atoms, or are they influenced by other nuclear spins such as that of the hydroperoxyl-H? Which γ-H (i.e., trans- or cis-vicinal to the O_2 group) yields the higher hfcc's that have been experimentally observed? Do the hfcc's arising from the individual conformational isomers of DMPO−O_2H differ?

Although DMPO is still widely employed as a spin trap, it has major drawbacks which include the short half-life of the $O_2^{\bullet-}$ adduct ($t_{1/2}$ = 60 s)[14−18] which limits the $O_2^{\bullet-}$ detection. Several DMPO-type analogues such as alkoxyphosphorylated nitrones[19−22] and alkoxycarbonyl-nitrones[23−29] have been developed by Tordo et al., and they demonstrated relatively longer half-lives ($t_{1/2}$ = 8−15 min) as compared with that of the DMPO−O_2H adduct. Although the development of substituted spin traps with longer half-lives is a significant improvement over DMPO, the basic understanding of the mechanism of DMPO−O_2H decay still remains unclear and is critical in the design of future spin traps with improved properties. In a companion paper,[30] we presented an analysis of the formation of the DMPO adducts with superoxide anion and hydroperoxyl radical. In this paper, we will address the thermodynamics and kinetic considerations of the decay of DMPO−O_2H. Herein, we report our theoretical efforts to answer these diverse questions.

II. Computational Methods

Density functional theory (DFT)[31,32] was applied in this study to determine the optimized geometry, vibrational frequencies, and single-point energy of all stationary points.[33−36] The effect of solvation on the gas-phase calculations was also investigated using the polarizable continuum model (PCM).[37−41] All calculations were performed using Gaussian 98[42] or Gaussian 03[43] at

* To whom correspondence should be addressed. E-mail: villamena-1@medctr.osu-edu (F.A.V.); hadad.1@osu.edu (C.M.H.); zweier-1@medctr.osu.edu (J.L.Z.). Fax: (614)-292-8454 (F.A.V.); (614)-292-1685 (C.M.H.); (614)-247-7799 (J.L.Z.).

† The Davis Heart and Lung Research Institute and College of Medicine.

‡ Department of Chemistry.

10.1021/jp0524330 CCC: $30.25
Published on Web 06/17/2005

the Ohio Supercomputer Center. Single-point energies were obtained at the B3LYP/6-31+G(d,p) level based on the optimized B3LYP/6-31G(d) geometries, unless otherwise indicated. The minima for both the nitrone spin traps and $O_2^{\bullet-}/^{\bullet}O_2H$ adducts have zero imaginary vibrational frequencies as derived from a vibrational frequency analysis (B3LYP/6-31G(d)). A scaling factor of 0.9806 was used[44] for the zero-point vibrational energy (ZPE) corrections. Spin contamination for all stationary points of the $O_2^{\bullet-}/^{\bullet}O_2H$ adduct structures was negligible, that is, $0.75 < \langle S^2 \rangle < 0.76$.

Calculation of Isotropic Hyperfine Coupling Constants. All quantum chemical calculations were performed using Gaussian 03.[43] Complexes of DMPO−O_2H with two water molecules were obtained stochastically via a series of computational methods. Spartan 04[45,46] was utilized to generate 18 DMPO−O_2H•$(H_2O)_2$ and 15 DMPO−OH•$(H_2O)_2$ complexes via a Monte Carlo method coupled with the MMFF-94 force field. The energetic window of accepted complexes was limited to fall within 10 kcal/mol of the lowest energy complex. Cases in which similar geometric and energetic parameters were obtained were then inspected visually. All unique complexes were subsequently optimized at the B3LYP/6-31G(d) level in the gas phase. The B3LYP optimized geometries were screened again for uniqueness. Each distinct complex was confirmed to be sufficiently converged and to be a minimum on the potential energy surface (PES) via vibrational frequency analysis at the B3LYP/6-31G(d) level. Converged minima were characterized by having all real vibrational frequencies. Complexes corresponding to saddle points (i.e., those having imaginary vibrational frequencies) were displaced (typically 10%) along the normal coordinate for the imaginary vibrational frequency in both directions and reoptimized via the opt=calcfc keyword. Reoptimized structures were analyzed for uniqueness and verified to be minima. The energy of each DMPO−OH and DMPO−O_2H conformation and their complexes was further refined via B3LYP/6-31+G(d,p)[34−36] single-point energy calculations using the scf=tight convergence criteria for both gas-phase and solution (water) energetics via the PCM model. Approximations to alleviate basis set superposition error (BSSE) at the B3LYP/6-31+G(d,p) level were determined using the counterpoise technique.[47,48] No effect was observed on the relative free energies and Boltzmann ratios with the counterpoise method. The Boltzmann ratios changed at most by 1% for the DMPO−O_2H•$(H_2O)_2$ complexes and by 0% for the DMPO−OH•$(H_2O)_2$ complex. As a result, the free energies, presented in this paper, are independent of the counterpoise correction for both the gas- and aqueous-phase calculations. Callam et al.[49] have shown that B3LYP/6-31+G(d,p) energies using a moderately sized basis set on HF or B3LYP geometries result in energetics that are in reasonable agreement with more expensive G2(MP2) and CBS-QB3 composite methods for the determination of conformational weightings for glycerol. Other comparisons of the quantitative and qualitative efficiency of the B3LYP method for predicting the properties of related *N*-oxyl radicals are discussed below. Specifically, the CBS-QB3 method was used for comparison purposes.[50,51] B3LYP/6-31G(d) zero-point vibrational energies were scaled by 0.9806.[44] All thermal corrections were determined using the harmonic oscillator, rigid rotor, and ideal gas approximations at 1.0 atm and 298.15 K.

The calculation of the hfcc's using the B3LYP density functional and basis sets, EPR-II and EPR-III,[52] and the core-valence correlation-consistent cc-pCVDZ[53] was performed in the gas and aqueous phases. The hfcc's were also predicted for the DMPO−OH•$(H_2O)_2$ and DMPO−O_2H•$(H_2O)_2$ complexes using the PBE0 functional[54] and the EPR-II basis set in the gas phase, while PBE0/6-31G(d) was also employed with the PCM method. Refer to the Supporting Information for a discussion of the predicted hfcc's using all of the levels of theory mentioned above other than the B3LYP/6-31+G(d,p)//B3LYP/6-31G(d) level which is presented and discussed in the text.

Boltzmann Weightings. For each DMPO−O_2H conformation, DMPO−O_2H•$(H_2O)_2$ and DMPO−OH•$(H_2O)_2$ system, a 298 K Boltzmann contribution was determined. The weighting of each structure was determined via a Boltzmann average, as shown in eq 1.

$$N_j = \frac{g_j e^{(-G_j/k_B T)}}{\sum_i g_i e^{(-G_i/k_B T)}} \quad (1)$$

In eq 1, G_i is the free energy at 298 K of structure i at the B3LYP/6-31+G(d,p)//B3LYP/6-31G(d) level including the counterpoise correction, relative to the structure with the lowest free energy set as zero, g_i is the structural degeneracy, k_B is Boltzmann's constant, and T is the temperature (298 K). For comparison with experiment, the hfcc's for each set of individual DMPO−O_2H and DMPO−OH conformers as well as their complexes with two individual water molecules were Boltzmann-weighted and summed according to both the B3LYP/6-31+G(d,p)//B3LYP/6-31G(d) gas-phase and solution (PCM, water) free energies at 298 K.

III. Prediction of the Isotropic Hyperfine Coupling Constant

Spectral analysis using the EPR simulation technique of superoxide adducts of DMPO,[14] 5-carbamoyl-5-methyl-1-pyrroline *N*-oxide (AMPO),[55] 5-ethoxycarbonyl-5-methyl-1-pyrroline *N*-oxide (EMPO),[27] and 5-diethoxyphosphoryl-5-methyl-1-pyrroline *N*-oxide (DEPMPO)[19] is important for the accurate interpretation of experimental spectra. The spectrum resulting from DMPO−O_2H has been the subject of debate over the years, since the difference of only one atom from DMPO−O_2H to DMPO−OH, that is, that of oxygen with no nuclear spin, results in a dramatic change in the spectral profiles. The commonly accepted hfcc assignments for the 12-line EPR spectrum of DMPO−O_2H are $a_N = 14.3$ G, $a_H^{\beta} = 11.7$, and $a_H^{\gamma} = 1.25$ G. As this manuscript was being prepared, Rosen et al.[56] suggested that the γ-splitting neither originates from the hydrogen atoms of C-3 or C-4 nor originates from the hydroperoxyl hydrogen but instead originates from the superposition of two conformers of DMPO−O_2H, as demonstrated experimentally and theoretically using a Hartree−Fock (HF) theory approach at the UHF/6-31++G(d,p) level. Since HF theory neglects electron correlation and may suffer from spin contamination, we performed DFT studies on the stable conformers of DMPO−O_2H to further investigate the nature of its hyperfine coupling constants (hfcc's). Furthermore, we explored the role of implicit and explicit solvation on the available conformations and the resulting hfcc values.

Methods for predicting the hfcc values of organic-based free radicals have shown that electronic, environmental, and vibrational effects contribute to the magnitude of the hfcc EPR parameters.[57] The prediction of spin densities and a_N on various compounds bearing a nitroxyl moiety, for example, nitronyl nitroxides,[58] pyrrolidine *N*-oxides,[59] and piperidine *N*-oxide,[60] has been reported by computational DFT methods. The direct proportionality of the nuclear spin population (density) (ρ_{rx}) with

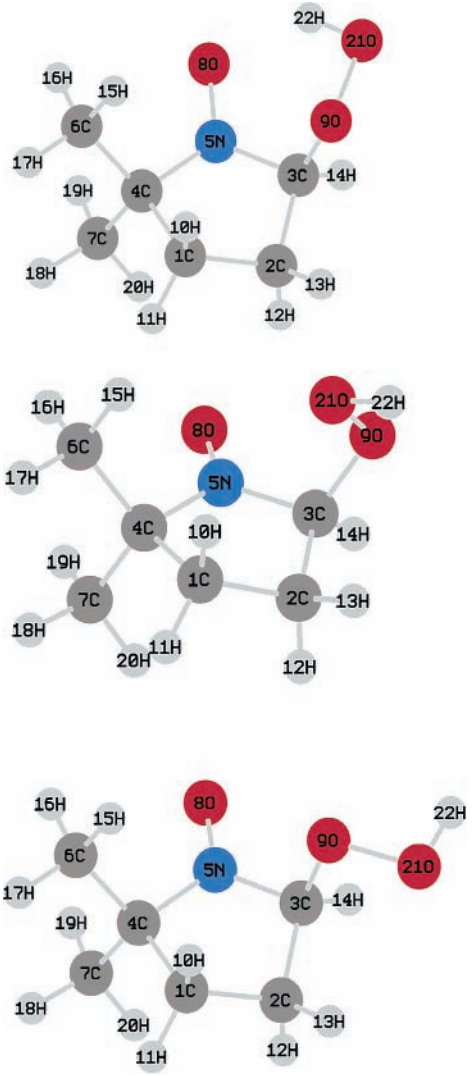

Figure 1. Graphical representation of the major A conformations A-1 (top), A-2 (middle), and A-3 (bottom) corresponding to *D*(N5−C3−O9−O21) angles (Θ) of 76.3, 173.0, and 294.0°, respectively.

a_X is based on eq 2:

$$a_X = 8\pi/3(g_e/g_0)\gamma_x\beta_x\rho_{rx} \qquad (2)$$

where g_0 is the isotropic g value for the radical, g_e is the g value for the free electron, γ_x is the gyromagnetic nuclear ratio, and β_x is the nuclear magneton of the nucleus X, and eq 2 allows us to calculate a_X of various adducts.[58]

The general conformation A has been chosen for the DMPO−O_2H adduct over conformation B as a model for the hfcc prediction due to its favored energetic preference in the gas and aqueous phases.[30]

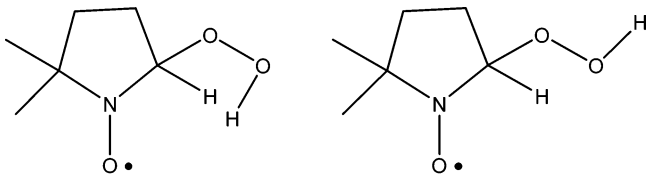

Conformer A **Conformer B**

Figure 1 shows three of the favored isomers of conformation A which were derived at the B3LYP/6-31+G(d,p)//B3LYP/6-31G-(d) level, that is, with *D*(N−C−O−O) dihedral angles of 75.9, 174.3, and 294.6°. These conformers, denoted as A-1, A-2, and A-3, respectively, were also optimized at the B3LYP/aug-cc-pVDZ level for comparison (see Supporting Information).[61] The geometry, spin population, and MO isosurface of the various A conformers are shown in Supporting Information Figures S1−S3 at the B3LYP/6-31+G(d,p)//B3LYP/6-31G(d) level. The computed spin densities ($\alpha-\beta$) using the natural population analysis (NPA) method[62] allows us to quantify the amount of spin population associated with each of the atoms. The quantitative (partitioned) NPA results (Table 1) are in good agreement with the spin population pictures (Supporting Information Figures S1−S3) which are based on the calculated wave functions, and not a particular partitioning technique. The γ-H of the methylene groups gave a relatively small, but non-negligible, contribution to the α-SOMO (see Supporting Information Figures S1d−S3d). However, the B3LYP spin population values of the γ-H based on Table 1 may not be significant, and therefore, we tabulated the theoretical hfcc in order to best compare to the experimental data.

TABLE 1: Spin Densities ($\alpha-\beta$, in Electrons) of Various Conformers of DMPO−O_2H from a Natural Population Analysis at the B3LYP/6-31+G(d,p)//B3LYP/6-31G(d) Level in the Gas and Aqueous (PCM) Phases

	excess alpha electron spin ($\alpha-\beta$)							
	B3LYP/6-31+G(d,p)				PCM/B3LYP/6-31+G(d,p)			
atom	A-1	A-2	A-3	Boltz.	A-1	A-2	A-3	Boltz.
C1	0.002	0.001	0.002	0.002	0.003	0.001	0.002	0.001
C2	0.001	0.001	−0.001	0.001	0.001	0.002	0.000	0.000
C3	−0.017	−0.014	−0.012	−0.017	−0.018	−0.016	−0.015	−0.015
C4	−0.022	−0.023	−0.024	−0.023	−0.023	−0.025	−0.025	−0.025
N5	0.459	0.403	0.410	0.456	0.488	0.449	0.464	0.461
C6	0.015	0.016	0.016	0.015	0.016	0.017	0.017	0.017
C7	0.021	0.021	0.024	0.021	0.023	0.023	0.026	0.025
O8	0.494	0.547	0.542	0.497	0.465	0.503	0.490	0.492
O9	0.036	0.024	0.026	0.035	0.035	0.024	0.027	0.026
H10	0.000	0.000	0.000	0.000	0.000	0.000	0.000	0.000
H11	0.001	0.000	0.000	0.001	0.001	0.000	0.000	0.000
H12	0.001	0.000	0.001	0.001	0.001	0.000	0.001	0.001
H13	0.000	0.003	0.002	0.000	0.000	0.003	0.002	0.002
H14	0.009	0.011	0.016	0.009	0.009	0.010	0.016	0.015
H15	0.000	0.000	0.000	0.000	0.000	0.000	0.000	0.000
H16	−0.001	−0.001	−0.001	−0.001	−0.001	−0.001	−0.001	−0.001
H17	0.000	0.000	0.000	0.000	0.000	0.000	0.000	0.000
H18	0.002	0.001	0.001	0.002	0.002	0.001	0.001	0.001
H19	−0.001	−0.001	−0.001	−0.001	−0.001	−0.001	−0.001	−0.001
H20	−0.001	−0.001	−0.001	−0.001	−0.001	−0.001	−0.001	−0.001
O21	0.005	0.012	0.000	0.005	0.004	0.012	0.000	0.003
H22	−0.002	0.000	0.000	−0.002	−0.002	0.000	0.000	0.000

On the basis of the seminal work of Barone and co-workers for calculating hfcc parameters for *N*-oxyl radicals,[59] we predicted the hfcc's of the three different conformers (A-1, A-2, and A-3) at the B3LYP/6-31+G(d,p)//B3LYP/6-31G(d) level for the isolated spin adduct in the gas phase (see Table 2). The B3LYP/6-31+G(d,p)//B3LYP/6-31G(d) level of theory has been employed previously[63] to predict a_N for various nitronyl nitroxides and found to be in good agreement with the experimental values. (We also explored other basis sets and functionals, and the results are very consistent; see the Supporting Information.)

Our results (Table 2) show that the best agreement with experiment for a_N can be found with conformer A-1 in the gas phase with predicted a_N = 11.87 G versus experimental a_N = 14.3 G. This Δa_N value of −2.43 G translates to a relative error of −17%. None of the conformers gave an accurate prediction of the a value for any of the γ-H's, but the closest value to the experimental one was achieved only from conformer A-1 with an error of −14% for the γ-H trans-vicinal (H-12) to the

TABLE 2: Predicted Gas- and Aqueous-Phase Isotropic Hyperfine Coupling Constants (hfcc's) and Corresponding Errors[a] of N, β-H, and γ-H[b] in Various Conformations of DMPO−O_2H Using the B3LYP/6-31G(d) Optimized Geometry

	isotropic hyperfine splitting constants, *a* (G)							
	B3LYP/6-31+G(d,p)//B3LYP/6-31G(d) DMPO−O_2H				PCM/B3LYP/6-31+G(d,p)//B3LYP/6-31G(d) DMPO−O_2H			
atom	A-1	A-2	A-3	Boltz.	A-1	A-2	A-3	Boltz.
N5	11.87	9.04	9.38	11.69	12.73	10.22	10.72	10.65
γ-*H10*	−0.34	−0.20	−0.19	−0.33	−0.35	−0.24	−0.25	−0.25
γ-*H11*	0.31	−0.25	−0.38	0.27	0.25	−0.31	−0.46	−0.42
γ-*H12*	1.07	0.70	0.81	1.05	1.15	0.66	0.70	0.70
γ-*H13*	0.42	1.84	1.80	0.51	0.47	1.84	1.82	1.81
β-*H14*	6.60	5.29	9.07	6.57	6.93	6.50	10.11	9.30
errors								
$\lvert a_{N5}\rvert/\lvert a_{H14}\rvert$[c]	1.8	1.71	1.03	1.78	1.84	1.57	1.06	1.14
$\Delta a_N(a_{N5})$	−2.43 (−17.0)	−5.26 (−36.8)	−4.92 (−34.4)	−2.61 (−18.3)	−1.57 (−11.0)	−4.08 (−28.5)	−3.58 (−25.0)	−3.65 (−25.5)
$\Delta a_H^{\gamma}(a_{H12})$	−0.18 (−14.4)	−0.55 (−44.0)	−0.44 (−35.2)	−0.2 (−16.0)	−0.1 (−8.0)	−0.59 (−47.2)	−0.55 (−44.0)	−0.55 (−44.0)
$\Delta a_H^{\gamma}(a_{H13})$	−0.83 (−66.4)	0.59 (47.2)	0.55 (44.0)	−0.74 (−59.2)	−0.78 (−62.4)	0.59 (47.2)	0.57 (45.6)	0.56 (44.8)
$\Delta a_H^{\beta}(a_{H14})$	−5.1 (−43.6)	−6.41(−54.8)	−2.63 (−22.5)	−5.13 (−43.8)	−4.77 (−40.8)	−5.2 (−44.4)	−1.59 (−13.6)	−2.4 (−20.5)

[a] $\Delta a_x = a_{calcd} - a_{exptl}$. Experimental values are $a_N = 14.3$ G, $a_{\beta\text{-H}} = 11.7$ G, and $a_{\gamma\text{-H}} = 1.25$ G. Values in parentheses are % error = $[(a_{calcd} - a_{exptl})/a_{exptl}] \times 100$. Negative values represent an underestimation of the experimental values, that is, $a_{calcd} < a_{exptl}$, while positive values represent an overestimation of the experimental values. [b] The γ-H is based on the H's with the two largest predicted hfcc values. [c] Experimental $\lvert a_N\rvert/\lvert a_{\beta\text{-H}}\rvert = 1.22$.

hydroperoxyl moiety. The γ-H's that are cis-vicinal (H-13) to the hydroperoxyl moiety in conformers A-2 and A-3 gave the highest hfcc compared to the other γ-H's in their respective molecules, consistent with the spin population plots shown in Supporting Information Figures S1−S3. However, in reality, each of these individual conformers will contribute to the observed EPR spectra based on their Boltzmann contribution. We, therefore, used the calculated, relative free energies of the different conformers to simulate a Boltzmann-weighted average of the theoretical hfcc values, and the resulting data (Table 2) are dominated by the A-1 conformer, since it is strongly preferred. The Boltzmann-averaged hfcc of the three conformers gave a reasonably predicted a_N value of 11.69 G but a poorly predicted value for a_H^{β} of 6.57 G compared to experimental values for a_N and a_H^{β} of 14.3 and 11.7 G, respectively. The highest Boltzmann-averaged a_H value was predicted from the trans-vicinal γ-H (H-12) of $a_H^{\gamma} = 1.05$ G close to the experimental value of 1.25 G.

The relative ΔG(298K) values (kilocalories per mole) (and Boltzmann weighting) at the B3LYP/6-31+G(d,p)//B3LYP/6-31G(d) level are as follows: A-1, 0.0 (0.93); A-2, 1.71 (0.05); A-3, 2.44 (0.02), while the values at the CBS-QBS level, for comparison, are the following: A-1, 0.0 (0.97); A-2, 2.35 (0.02); A-3, 2.39 (0.02). The overall effect of the level of theory, that is, B3LYP/6-31+G(d,p)//B3LYP/6-31G(d) versus CBS-QB3, on the Boltzmann-weighted hfcc's for the three gas-phase DMPO−OOH conformations is negligible. The relative free energy values only change significantly for the A-2 conformer at the CBS-QB3 level.

We also considered the influence of environmental effects on the hfcc values for these conformers. Solvation effects have been shown to affect the isotropic hfcc of nitrogen in nitroxides by 2.5 G when going from nonpolar solvents to water.[57] We, therefore, hypothesized that the poorly predicted hfcc in the gas phase may be improved by including some representation of the bulk solvent effect using a PCM[37−41] calculation. It has been demonstrated for five- and six-membered-ring nitroxides that the computed a_N values gave good agreement with the experimental values when solvation was considered.[60] Table 2 shows the differences, relative to experiment, for the calculated a_N, a_H^{β}, and a_H^{γ} values using single-point energy calculations with the PCM method and water as a solvent. For the individual conformers, the PCM method does generally increase the predicted hfcc and brings the values closer to the experimental values for N, β-H, and γ-H. Improved values are more evident for a_N and a_H^{β}. However, since the A-1 conformer is reduced in energetic preference at the PCM level, the Boltzmann-averaged values for the relevant hfcc's showed improvement only for a_H^{β} and a_H^{γ} (H-13) but gave a poorer a_N value of 10.65 G.

We then focused our attention on the effect of explicit H-bonding between the solvent (in this case, water) and the nitroxide moiety on the resulting hfcc values. It has been demonstrated that the addition of explicit interactions from water molecules to nitroxides through H-bonding as well as taking into consideration the bulk contribution of the solvent can almost quantitatively predict the hfcc of N at the PCM/PBE0/6-31G(d) level.[60] (Results for the predicted hfcc values at the PBE0/6-31G(d) level are discussed, relative to the B3LYP data, and provided in the Supporting Information). We considered the effect of H-bonding by two water molecules on the calculated hfcc in the gas phase at the B3LYP/6-31+G(d,p)//B3LYP/6-31G(d) level of theory. In this study, the DMPO−OH adduct was also considered to provide additional insights into the nature of the γ-H hfcc of DMPO−O_2H.

Using a stochastic approach (see the methods section), we generated a structurally diverse set of ring conformations and water coordination for the DMPO adducts with OH and O_2H. From the sets of 18 unique DMPO−O_2H•$(H_2O)_2$ and 15 unique DMPO−OH•$(H_2O)_2$ complexes, two conformers dominated the 298 K Boltzmann distributions and contributed >98%. These structures are shown in Figure 2. For DMPO−O_2H•$(H_2O)_2$, the ratio of the two stable complexes is 2.7:1 for complex 1/complex 2, while, for DMPO−OH•$(H_2O)_2$, the ratio is 2.5:1 for complex 1/complex 3. The most favored two-water DMPO-X (X = OH or O_2H) complexes involve a two-water bridge with one water coordinated with the hydrogen of the O_2H or OH group via the first water's oxygen and a hydrogen donated to the second water's oxygen. The second water also donates a hydrogen to the nitroxide moiety's oxygen. The two most favored complexes for each set have the same water arrangement and differ only in ring conformation. The lowest energy complex in each set has the $^2T_3$ twist conformation in which the carbon with the X moiety is designated as number 1 (Scheme 1). Only structures in the southern hemisphere of the pseudorotational itinerary[64−67] for the five-membered ring are favored.

The hfcc's[68] of DMPO−O_2H•$(H_2O)_2$ are shown in Table 3 as derived at the B3LYP/6-31+G(d,p)//B3LYP/6-31G(d) level.

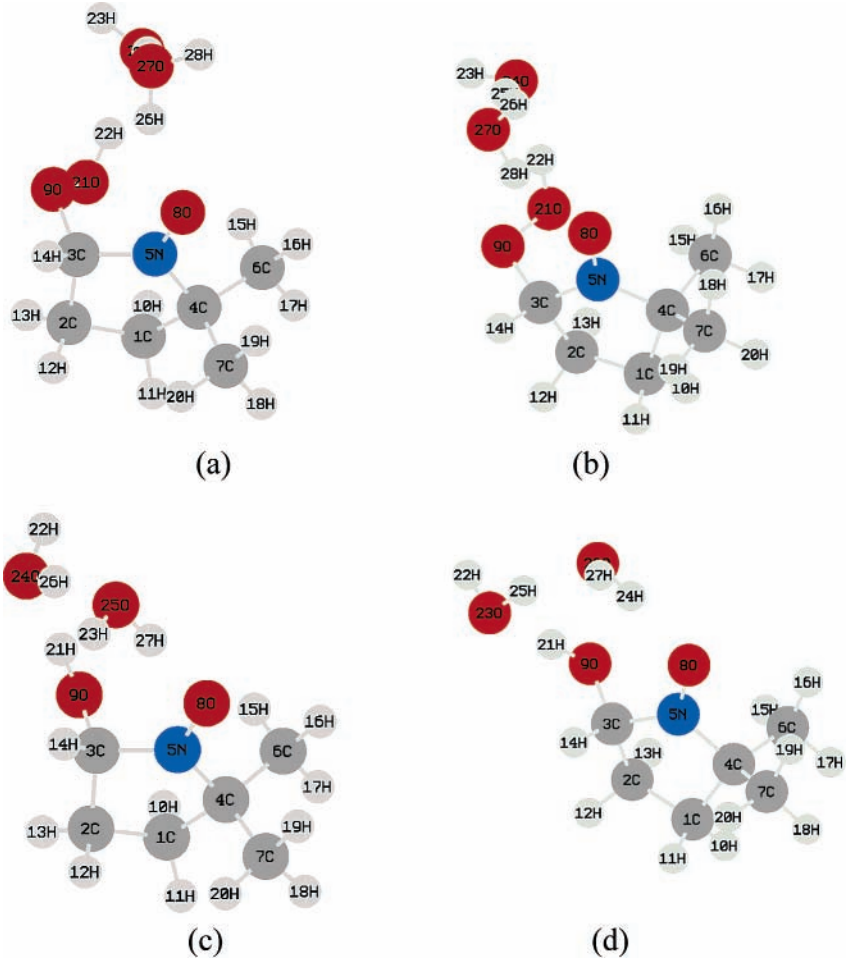

Figure 2. View of the B3LYP/6-31G(d) optimized structures of complex 1 (a) and complex 2 (b) of DMPO−O_2H and complex 1 (c) and complex 3 (d) of DMPO−OH as coordinated with two explicit water molecules.

SCHEME 1

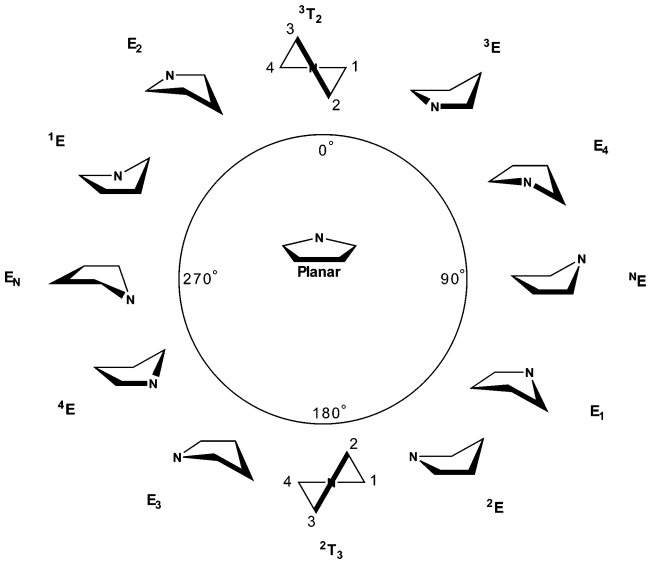

Better agreement of the predicted hfcc's of the β-H and γ-H with the experimental values has been achieved for complex 1 of DMPO−O_2H•(H_2O)$_2$. The predicted hfcc's for β-H and γ-H for complex 1 were below 12% error, but a_N was underestimated by as much as 22%, while the ratio of a_N to a_H^β is 1.07 which is comparable to the experimental ratio of 14.3/11.4 = 1.25. The predicted hfcc for the γ-H of complex 2, however, showed similar results in predicting a_N but gave a poorer approximation of a_H^β and a_H^γ, that is, 40 and 83% error, respectively. Use of the Boltzmann-averaged hfcc's for complexes 1 and 2 did not improve the relative error for a_N but gave very good agreement for a_H^γ with −18% error for the cis-vicinal H-13 and almost quantitative prediction for a_H^β with 2.9% error. Therefore, optimization in the gas phase of complex 1 of DMPO−O_2H using two explicit water molecules can predict a_H^β and a_H^γ with relatively good accuracy (less than 12% error), while accurate prediction of a_N was not achieved.

As shown in Table 4, the two adduct complexes for DMPO−OH•(H_2O)$_2$ have significantly different hfcc's for several atoms, likely resulting from different ring orientations, $^2T_3$ versus $^3T_2$. Only small adjustments are made to accommodate the change of ring pucker between the $^2T_3$ and $^3T_2$ conformations. The predicted hfcc for a_N in complexes 1 and 3 of DMPO−OH•(H_2O)$_2$ gave values of 12.38 and 12.04 G, respectively. These values translate to underestimated errors of about −17 to −19% (Table 4). The a_H^β value was underestimated by as much as ∼−72% in complex 1 but was overestimated by ∼24% in complex 3. Complex 3 yielded good predicted results for a_H^γ at all levels of theory but not for complex 1 in which two γ-H's (i.e., H-12 and H-13) gave significant hfcc's (1.47−1.70 G). Considering that complex 1 contributes about 70% to the Boltzmann average and large deviations of the hfcc are predicted compared to the experimental values, the experimentally observed hfcc is most probably a result of fast exchange between the isomeric forms. Therefore, proper averaging of the hfcc values from two or more conformational isomers may be necessary to reproduce the

TABLE 3: Predicted Gas- and Aqueous-Phase Isotropic Hyperfine Coupling Constants (hfcc's) and Corresponding Errors[a] of N, β-H, and γ-H[b] in the Complexes of DMPO−O_2H with Two Explicit Water Molecules Using the B3LYP/6-31G(d) Optimized Geometry

	isotropic hyperfine splitting constants, *a* (G)					
	B3LYP/6-31+G(d,p)//B3LYP/6-31G(d) DMPO−O_2H•$(H_2O)_2$			PCM/B3LYP/6-31+G(d,p)//B3LYP/6-31G(d) DMPO−O_2H•$(H_2O)_2$		
atom	complex 1	complex 2	Boltzmann-weighted	complex 1	complex 2	Boltzmann-weighted
N5	11.09	11.42	10.62	11.54	12.02	11.76
γ-H10	−0.29	0.53	−0.07	−0.31	0.55	0.09
γ-H11	−0.34	−0.23	−0.30	−0.39	−0.26	−0.33
γ-H12	0.73	−0.05	0.50	0.74	−0.09	0.35
γ-H13	1.38	0.21	1.02	1.44	0.16	0.84
β-H14	10.33	16.51	11.36	10.62	17.01	13.62
errors						
$\lvert a_{N5}\rvert/\lvert a_{H14}\rvert$[c]	1.07	0.69	0.93	1.09	0.71	0.86
$\Delta a_N(a_{N5})$	−3.21 (−22.4)	−2.88 (−20.1)	−3.68 (−25.7)	−2.76 (−19.3)	−2.28 (−15.9)	−2.54 (−17.8)
$\Delta a_H^{\gamma}(a_{H12})$	−0.52 (−41.6)	−1.3 (−104.0)	−0.75 (−60.0)	−0.51 (−40.8)	−1.34 (−107.2)	−0.9 (−72.0)
$\Delta a_H^{\gamma}(a_{H13})$	0.13 (10.4)	−1.04 (−83.2)	−0.23 (−18.4)	0.19 (15.2)	−1.09 (−87.2)	−0.41 (−32.8)
$\Delta a_H^{\beta}(a_{H14})$	−1.37 (−11.7)	4.81 (41.1)	0.34 (2.9)	−1.08 (−9.2)	5.31 (45.4)	1.92 (16.4)

[a] $\Delta a_x = a_{calcd} - a_{exptl}$. Experimental values are $a_N = 14.3$ G, $a_{\beta\text{-H}} = 11.7$ G, and $a_{\gamma\text{-H}} = 1.25$ G. Values in parentheses are % error $= [(a_{calcd} - a_{exptl})/a_{exptl}] \times 100$. Negative values represent an underestimation of the experimental values, that is, $a_{calcd} < a_{exptl}$, while positive values represent an overestimation of the experimental values. [b] The γ-H is based on the H's with the two largest predicted hfcc values. [c] Experimental $\lvert a_N\rvert/\lvert a_{\beta\text{-H}}\rvert = 1.22$.

TABLE 4: Predicted Gas- and Aqueous-Phase Isotropic Hyperfine Coupling Constants (hfcc's) and Corresponding Errors[a] of N, β-H, and γ-H[b] in the Complexes of DMPO−OH with Two Explicit Water Molecules Using the B3LYP/6-31G(d) Optimized Geometry

	isotropic hyperfine splitting constants, *a* (G)					
	B3LYP/6-31+G(d,p)//B3LYP/6-31G(d) DMPO−OH•$(H_2O)_2$			PCM/B3LYP/6-31+G(d,p)//B3LYP/6-31G(d) DMPO−OH•$(H_2O)_2$		
atom	complex 1	complex 3	Boltzmann-weighted	complex 1	complex 3	Boltzmann-weighted
N5	12.38	12.04	11.96	13.00	12.67	12.89
γ-H10	−0.30	0.37	−0.10	−0.31	0.35	−0.08
γ-H11	−0.30	−0.23	−0.27	−0.33	−0.26	−0.31
γ-H12	1.47	−0.03	1.01	1.50	−0.07	0.96
γ-H13	1.70	0.11	1.21	1.78	0.36	1.29
β-H14	4.12	18.44	8.02	4.29	19.16	9.38
errors						
$\lvert a_{N5}\rvert/\lvert a_{H14}\rvert$[c]	3.00	0.65	1.49	3.03	0.66	1.37
$\Delta a_N(a_{N5})$	−2.52 (−16.9)	−2.86 (−19.2)	−2.94 (−19.7)	−1.90 (−12.8)	−2.23 (−15.0)	−2.01 (−13.5)
$\Delta a_H^{\gamma}(a_{H12})$	1.47	−0.03	1.01	1.5	−0.07	0.96
$\Delta a_H^{\gamma}(a_{H13})$	1.7	0.11	1.21	1.78	0.36	1.29
$\Delta a_H^{\beta}(a_{H14})$	−10.78 (−72.3)	3.54 (23.8)	−6.88 (−46.2)	−10.61 (−71.2)	4.26 (28.6)	−5.52 (−37.0)

[a] $\Delta a_x = a_{calcd} - a_{exptl}$. Experimental values are $a_N = 14.9$ G and $a_{\beta\text{-H}} = 14.9$ G. Values in parentheses are % error $= [(a_{calcd} - a_{exptl})/a_{exptl}] \times 100$. Negative values represent an underestimation of the experimental values, that is, $a_{calcd} < a_{exptl}$, while positive values represent an overestimation of the experimental values. [b] The γ-H is based on the H's with the two largest predicted hfcc values. [c] Experimental $\lvert a_N\rvert/\lvert a_{\beta\text{-H}}\rvert = 1.00$.

experimental hfcc of the DMPO−OH•$(H_2O)_2$ adduct. In fact, the Boltzmann-weighted average hfcc values seem to improve the values for a_N and a_H^{β} as well as their ratio compared to the hfcc's of the individual complexes.

Hence, we then investigated the additive effect of the dielectric effect of the solvent together with the effect of explicit H-bonding interactions with the solvent molecules. We anticipated improvement for the hfcc of the adduct molecules, as was demonstrated by Saracino et al.[60] at the PCM/PBE0/6-31G(d) level on 2-carboxy-PROXYL (CP).[69] For consistency with the previous methods used, results from the optimized structures at the B3LYP/6-31G(d) level will be discussed in this section. A comparison of the predicted hfcc's of the DMPO−O_2H•$(H_2O)_2$ and DMPO−OH•$(H_2O)_2$ complexes optimized in the gas and aqueous phases is shown in Tables 3 and 4. In general, there is only about 0.6 G improvement in the predicted a_N values for DMPO−OH and DMPO−O_2H when the dielectric field of the bulk solvent is considered. Higher a_H^{β} values were predicted for both adducts when the calculation was carried out in the presence of the solvent's dielectric field in conjunction with explicit water molecules.

Boltzmann averaging of all of the pertinent hfcc's for DMPO−O_2H•$(H_2O)_2$ showed an overestimation of a_H^{β} (by 14%) and an underestimation of a_H^{γ} (by 18%) at the PCM level as compared to the gas phase, while a_N is slightly improved to about −18% error in the presence of the solvent's dielectric field. No significant change in the a_H^{γ} values was seen from DMPO−OH•$(H_2O)_2$ in the presence of the solvent's dielectric field.

Overall, prediction of a_N, a_H^{β}, and a_H^{γ} from DMPO−O_2H•$(H_2O)_2$ at the B3LYP/6-31+G(d,p)//B3LYP/6-31G(d) level using Boltzmann-averaged values gave reasonably good agreement with the experimental hfcc's when taking into account the dielectric field of the bulk solvent as well as the explicit H-bond potential of water molecules with the adduct. The Boltzmann-averaged hfcc values for the two DMPO−OH•$(H_2O)_2$ complexes also gave good agreement with the experimental values, specifically lowering the a_N to a_H^{β} ratio from 1.49 to 1.37.

We have reasonably predicted the hfcc's of the relevant nuclei and shown that the Boltzmann-averaged values are in good agreement with experiment. We should add that other factors

may also influence the hfcc values, such as dynamic effects due to the variation of a_N induced by the low-frequency inversion motion of the nitrogen atom due to the degree of pyramidalization of the nitroxide moiety (an error of approximately 1 G),[70] and perhaps due to the exchange interaction from neighboring adducts. However, in all of the models used here, we computed no significant hfcc contribution from the hydroperoxyl-H or the hydroxyl-H of DMPO−O_2H and DMPO−OH, respectively, consistent with the reported[56] spin-trapping experiment of $O_2^{\bullet-}$ in D_2O showing no difference in the EPR spectra of DMPO−O_2H and DMPO−O_2D. The γ-H cis-vicinal to the hydroperoxyl or hydroxyl moieties (i.e., H-13) gave the highest hfcc compared to the rest of the γ-H's in the adducts, and the fluxional role of the different conformations and complexes provided the averaged spectral parameters that compare well to experiment.

IV. Thermodynamics of DMPO−O_2H Adduct Decomposition

This section will focus only on the spontaneity of decomposition of the DMPO−O_2H adduct in the gas phase at the B3LYP/6-31+G(d,p)//B3LYP/6-31G(d) level. An EPR study showed that DMPO−O_2H undergoes decomposition to give DMPO−OH.[16] Although the actual mechanism of DMPO−O_2H decomposition has not been given much attention, there are indirect studies that could aid in the elucidation of the relevant mechanism. For example, the decomposition of nitroxyls, O−N(CHMe$_2$)CMe$_3$ and O−N(CDMe$_2$)CMe$_3$, indicates a bimolecular reaction with C−H$^\beta$ bond rupture in the slow step of the decomposition.[71] Further evidence of this process has been provided by stabilization of a nitroxyl adduct bearing a β-H through complexation to an Lewis acidic transition metal ion or decomposition to a nitrone in the presence of a relatively weakly Lewis acidic metal ion such as Zn^{2+}.[72] Moreover, superoxide adducts lacking a β-H have exhibited enhanced stability as compared to DMPO−O_2H.[15] The half-lives of DMPO−OH[73] or DMPO−O_2H adducts[16,74] at basic pH are significantly shorter than those at neutral or acidic pH. Sankuratri et al.[75] proposed a different mechanism in which the instability of the DMPO−OH and DMPO−O_2H adducts at basic pH is due to the initial abstraction of the hydroperoxyl-H; however, kinetic studies are not available to support this mechanism.

Recent theoretical studies on the decomposition of the DMPO−OH adduct revealed that the charge density distribution at C−H$^\beta$ does not vary for spin adducts with different substituents.[76] However, the charge density on the nitroxyl-N does vary significantly depending on the nature of the substituents attached to the C-5 position. This may indicate that the C(2)−N bond-breaking process may play a crucial role in the stability of spin adducts. Kramtsov et al.[77] have proposed a common decomposition product (*N*-hydroxy-pyrrolidone) for DEPMPO−O_2H and DEPMPO−OH adducts and noted that DEPMPO−O_2H undergoes decomposition via the formation of DEPMPO−OH, as evidenced by its EPR spectrum over a period of time.

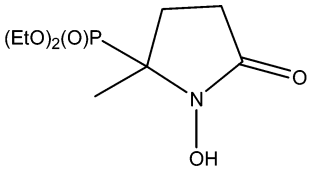

N-hydroxy-pyrrolidone

Experimental studies of DMPO−O_2H decay have indicated that only first-order kinetics occurs in aqueous solution.[29,74]

SCHEME 2

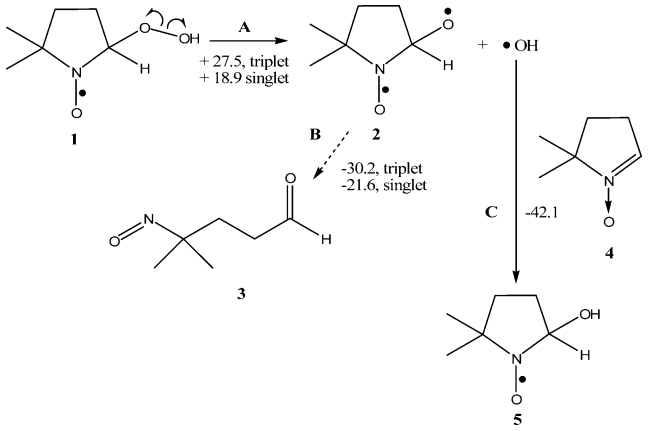

SCHEME 3

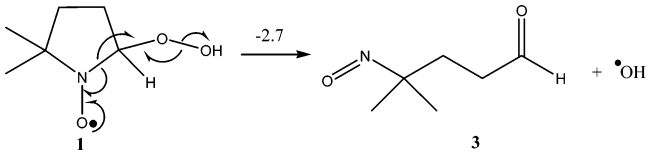

SCHEME 4

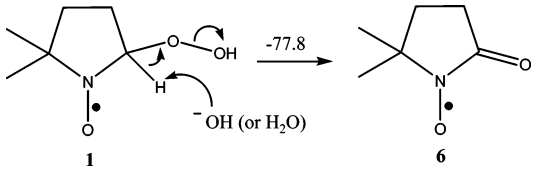

SCHEME 5

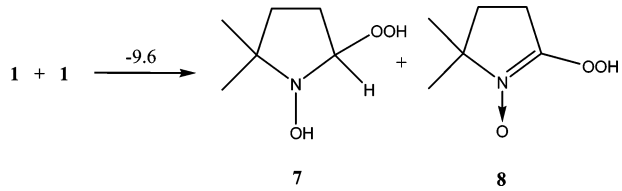

There are several possible mechanisms for this unimolecular decomposition, one of which involves homolytic bond breaking of the hydroperoxyl O−O bond[17] of **1** to form **2** (in triplet or singlet states) and subsequent trapping of the cleaved OH radical with DMPO (**4**) to form the hydroxyl adduct **5**, as shown in Scheme 2. $\Delta G_{rxn,298K}$ of the O−O bond-breaking process is endoergic by 27.5 and 18.9 kcal/mol for the formation of the triplet or (closed-shell) singlet states, respectively. Attempts to locate an open-shell singlet structure for **2** provided a preferred closed-shell solution. Conversion of **2** to nitrosoaldehyde (**3**) is exoergic with reaction free energies of −30.2 (from triplet **2**) and −21.6 kcal/mol (from singlet **2**). This provides a total free energy of −2.7 kcal/mol for the overall conversion of **1** to **3** via intramolecular rearrangement which involves a N−C bond cleavage with the elimination of •OH (Scheme 3).

As previously observed,[15,71,72,78] C−H$^\beta$ bond cleavage might occur during the unimolecular decomposition of DMPO−O_2H (**1**). As shown in Scheme 4, this reaction is highly favorable with a reaction free energy of −77.8 kcal/mol compared to the endoergic O−O bond cleavage reaction in Scheme 2. Although there is no kinetic evidence for the bimolecular decomposition of DMPO−O_2H (**1**) with itself to form **7** and **8** (Scheme 5), we nevertheless calculated the thermodynamics of this process and predicted this process to be also exoergic by −9.6 kcal/mol. However, on the basis of the relatively small concentration of

TABLE 5: Reaction Free Energies (kcal/mol) of Various Decomposition Pathways of DMPO−OOH and DEPMPO−OOH in the Gas and Aqueous Phases (in Parentheses)[a] at the B3LYP/6-31+G(d,p)//B3LYP/6-31G(d) Level

reaction scheme	DMPO−OOH	DEPMPO−OOH
scheme 2		
A (triplet)	27.5 (22.9)	28.8 (18.7)
(singlet)	18.9 (12.9)	−1.4 (−11.5)
B (triplet)	−30.2 (−29.2)	−30.7 (−24.8)
(singlet)	−21.6 (−19.2)	−0.5 (5.4)
scheme 3	−2.7 (−6.2)	−1.9 (−6.1)
scheme 4	−77.8 (−85.3)	−76.4 (−84.4)

[a] At the PCM/B3LYP/6-31+G(d,p)//B3LYP/6-31G(d) level using the gas-phase geometry.

SCHEME 6

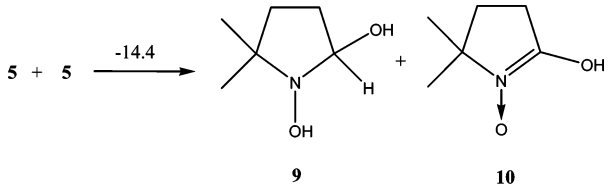

9 **10**

the radical adducts generated in experimental studies, it is quite unlikely, though energetically favorable, for this bimolecular reaction to be observed.

To validate our theoretical data, the thermodynamics of DEPMPO−OOH decay was investigated, since the first-order half-life of the decomposition of DEPMPO−OOH is ∼14 min compared to DMPO−OOH of ∼1 min. On the basis of the assumption that this unimolecular decomposition proceeds via N−C bond cleavage to form the nitrosoaldehyde and hydroxyl radical, we have calculated this process on the basis of the most preferred conformations for DEPMPO−OOH and its corresponding decomposition products (Table 5). It is clear that there is no significant difference in the overall energetics of decay of DMPO−OOH compared to DEPMPO−OOH (via Scheme 3 or 5) in both the gas and aqueous phases. However, a stepwise examination of the decay (based on Scheme 2) shows that there is a significant difference in the energetics of decay between DMPO−OOH and DEPMPO−OOH to their corresponding nitrosoaldehyde products (step B) via the formation of a biradical intermediate (step A). Although the formation of the biradical intermediate **2** has not been experimentally observed, we predict that the formation of the singlet species via homolytic cleavage of the O−O bond of the hydroperoxyl moiety is more thermodynamically preferred for DEPMPO−OOH compared to that of DMPO−OOH in an aqueous solution, but the subsequent decay of the singlet DEPMPO−O• intermediate to the nitrosoaldehyde is less favored (5.4 kcal/mol) compared to the singlet DMPO−O• (−19.2 kcal/mol). It is probable that the rate-limiting step (based on the experimental first-order kinetic data) is the formation of nitrosoaldehyde from an intermediate species.

The formation of DMPO−OH (**5**) from DMPO−O_2H (**1**) is commonly encountered in most EPR spin-trapping experiments (Scheme 2).[16] However, the exact mechanism by which this occurs is not clear at the moment, although kinetic data[29,74] suggest that the decomposition of DMPO−O_2H (**1**) has a first-order kinetic profile. So far, the formation of a nitroxyl-ketone (**6**), as shown in Scheme 4, is the most exoergic pathway for the unimolecular decomposition of **1**, but this could not explain the formation of **5** as observed experimentally. Nevertheless, although the ring-opening pathway (Scheme 3) may be less exoergic compared to the formation of **6** (Scheme 4), the former is a more plausible route for the formation of DMPO−OH. The effect of a dielectric field of the bulk solvent on the energetics of the decomposition of DMPO−O_2H (**1**) was considered, and the same trends are seen at the PCM level as in the gas phase. However, the exoergicities are even more enhanced in solvent, that is, −6.2 and −85.3 kcal/mol via the pathways shown in Schemes 3 and 4, respectively.

SCHEME 8

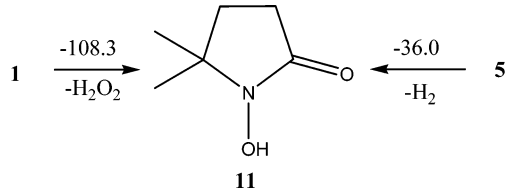

11

SCHEME 9

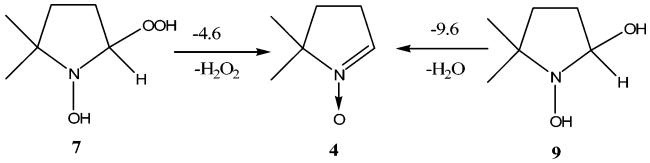

7 **4** **9**

The reaction described in Scheme 6 is considerably more exoergic than the bimolecular reaction of adduct **1** in Scheme 5. It has been previously proposed[76] that the cleavage of the nitroxyl C−N bond could be a contributing factor during the unimolecular decomposition of the DMPO−OH (**5**) adduct. Results show that the formation of a nitroxyl-aldehyde from **5** via heterolytic cleavage of the C−N bond based on Scheme 7 is only endoergic by 7.9 kcal/mol.

The formation of the *N*-hydroxy ketone (**11**) (which is analogous to that proposed by Kramtsov et al. as a common decomposition product from DEPMPO−O_2H or DEPMPO−OH)[77] and H_2O_2 from the decomposition of 2 mol of **1** was highly exoergic with a free energy of reaction of −108.3 kcal/mol, while the formation of **11** from **5** with the evolution of H_2 gas gave a free energy of reaction of −36.0 kcal/mol (see Scheme 8). A ^{31}P NMR study[77] showed that DEPMPO is recycled either from the $O_2^{\bullet-}$/•O_2H or the •OH adducts of DEPMPO via the formation of the corresponding hydroxylamine. Since the bimolecular decompositions of **1** or **5** (Scheme 5 or 6, respectively) are thermodynamically favorable, the formation of DMPO from the corresponding hydroxylamine **7** or **9** may also occur. We predicted that the conversion of **7** (with the formation of H_2O_2) or **9** (with the formation of H_2O) to **4** is exoergic with a free energy of reaction of −4.6 or −9.6 kcal/mol, respectively (Scheme 9).

Furthermore, it is also probable that the formation of **11** from **1** or **5** occurs via the formation of the nitrone−O_2H or −OH adducts **8** or **10** (see Scheme 10), as demonstrated by a previous

SCHEME 7

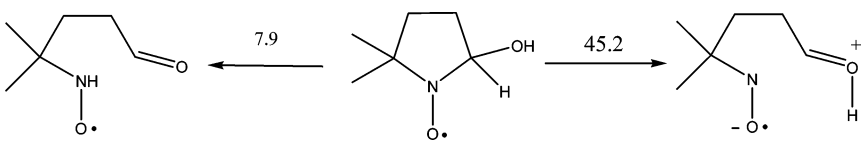

SCHEME 10

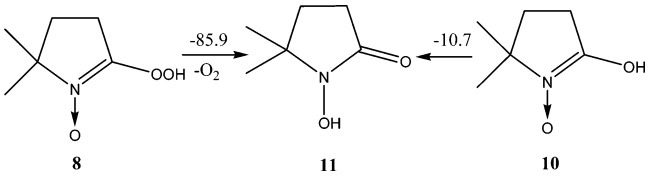

^{31}P NMR study[77] for an analogous reaction with DEPMPO. Reaction free energies for the formation of **11** were found to be exoergic with $G_{rxn,298K} = -85.9$ kcal/mol for **8** (from bimolecular decomposition of **8** with the evolution of O_2 gas) and −10.7 kcal/mol for **10**.

V. Conclusions

The isotropic hyperfine coupling constants of DMPO−O_2H, particularly those of N, β-H, and γ-H, were reasonably well predicted at the B3LYP/6-31+G(d,p)//B3LYP/6-31G(d) level by taking into account the explicit H-bonding of two water molecules to a Boltzmann-weighted average of the calculated conformations and complexes of the DMPO−O_2H adduct and also the bulk dielectric effect of the solvent. The γ-H cis-vicinal to the hydroperoxyl moiety gives rise to the highest hfcc compared to the other γ-H's. The hydroperoxyl proton did not give a significant hfcc. Prediction of the experimental hfcc of DMPO−OH requires conformational averaging of the preferred conformations available to this flexible molecule.

Decomposition of DMPO−O_2H can occur according to the following mechanisms in the order of decreasing favorability: β-H abstraction to a keto-nitroxide > bimolecular decomposition to form the corresponding nitrone and hydroxylamine > unimolecular ring opening to form a nitrosoaldehyde plus a hydroxyl radical. These calculations are consistent with the experimental kinetic data indicating that the decay of DMPO−O_2H involves both first- and second-order decay kinetics. However, only the unimolecular decomposition of the DMPO−O_2H adduct via the formation of nitrosoaldehyde (**3**), with concomitant generation of a hydroxyl radical (Scheme 3), can explain the formation of DMPO−OH observed experimentally during the decay of the DMPO−O_2H adduct. The bimolecular decomposition of DMPO−OH was also found to be thermodynamically favorable by forming the corresponding nitrone and hydroxylamine.

Acknowledgment. The authors wish to thank The Ohio Supercomputer Center (OSC) for support of this research and Prof. DeLanson R. Crist (Georgetown) and Dr. Micheal Bartberger (Amgen) for valuable suggestions. This work was supported by NIH grants HL38324, HL63744, and HL65608. C.M.H. acknowledges support from the NSF-funded Environmental Molecular Science Institute (CHE-0089147). J.K.M. acknowledges support from an Amoco fellowship.

Supporting Information Available: Energies, enthalpies, and free energies for all spin traps and their corresponding spin adducts and complete refs 42, 43, and 46. This material is available free of charge via the Internet at http://pubs.acs.org.

References and Notes

(1) Yamakoshi, Y.; Sueyoshi, S.; Fukuhara, K.; Miyata, N.; Masumizu, T.; Kohno, M. *J. Am. Chem. Soc.* **1998**, *120*, 12363−12364.
(2) Makino, K.; Mossoba, M. M.; Riesz, P. *J. Am. Chem. Soc.* **1982**, *104*, 3537−3539.
(3) Stoyanovsky, D. A.; Clancy, R.; Cederbaum, A. I. *J. Am. Chem. Soc.* **1999**, *121*, 5093−5094.
(4) Jones, C. M.; Burkitt, M. J. *J. Am. Chem. Soc.* **2003**, *125*, 6946−6954.
(5) Pryor, W. A.; Terauchi, K.; Davis, W. H. J. *Environ. Health Perspect.* **1976**, *16*, 161−176.
(6) Pou, S.; Pou, W. S.; Bredt, D. S.; Snyder, S. H.; Rosen, G. M. *J. Biol. Chem.* **1992**, *267*, 24173−24176.
(7) Harbour, J. R.; Bolton, J. R. *Biochem. Biophys. Res. Commun.* **1975**, *64*, 803−807.
(8) Xia, Y.; Zweier, J. L. *Proc. Natl. Acad. Sci. U.S.A.* **1997**, *94*, 6954−6958.
(9) Rosen, G. M.; Britigan, B. E.; Cohen, M. S.; Ellington, S. P.; Barber, M. J. *Biochim. Biophys. Acta* **1988**, *969*, 236−241.
(10) Chamulitrat, W.; Hughes, M. F.; Eling, T. E.; Mason, R. P. *Arch. Biochem. Biophys.* **1991**, *290*, 153−159.
(11) Zweier, J. L. *J. Biol. Chem.* **1988**, *263*, 1353−1357.
(12) Zweier, J. L.; Kuppusamy, P.; Lutty, G. A. *Proc. Natl. Acad. Sci. U.S.A.* **1988**, *85*, 4046−4050.
(13) Halliwell, B.; Gutteridge, J. M. C. *Free Radicals in Biology and Medicine*; Oxford Univeristy Press: Oxford, U.K., 1999.
(14) Finkelstein, E.; Rosen, G. M.; Rauckman, E. J. *J. Am. Chem. Soc.* **1980**, *102*, 4995.
(15) Finkelstein, E.; Rosen, G. M.; Rauckman, E. J. *Mol. Pharm.* **1979**, *16*, 676−685.
(16) Buettner, G. R.; Oberley, L. W. *Biochem. Biophys. Res. Commun.* **1978**, *83*, 69−74.
(17) Finkelstein, E.; Rosen, G. M.; Rauckman, E. J. *Mol. Pharm.* **1982**, *21*, 262−265.
(18) Pou, S.; Hassett, D. J.; Britigan, B. E.; Cohen, M. S.; Rosen, G. M. *Anal. Biochem.* **1989**, *177*, 1−6.
(19) Frejaville, C.; Karoui, H.; Tuccio, B.; Le Moigne, F.; Culcasi, M.; Pietri, S.; Lauricella, R.; Tordo, P. *J. Med. Chem.* **1995**, *38*, 258−265.
(20) Liu, K. J.; Miyake, M.; Panz, T.; Swartz, H. *Free Radical Biol. Med.* **1999**, *26*, 714−721.
(21) Stolze, K.; Udilova, N.; Nohl, H. *Free Radical Biol. Med.* **2000**, *29*, 1005−1014.
(22) Chalier, F.; Tordo, P. *J. Chem. Soc., Perkin Trans. 2* **2002**, 2110−2117.
(23) Olive, G.; Mercier, A.; Le Moigne, F.; Rockenbauer, A.; Tordo, P. *Free Radical Biol. Med.* **2000**, *28*, 403−408.
(24) Zhang, H.; Joseph, J.; Vasquez-Vivar, J.; Karoui, H.; Nsanzumuhire, C.; Martasek, P.; Tordo, P.; Kalyanaraman, B. *FEBS Lett.* **2000**, *473*, 58−62.
(25) Stolze, K.; Udilova, N.; Nohl, H. *Biol. Chem.* **2002**, *383*, 813−820.
(26) Stolze, K.; Udilova, N.; Rosenau, T.; Hofinger, A.; Nohl, H. *Biol. Chem.* **2003**, *384*, 493−500.
(27) Tsai, P.; Ichikawa, K.; Mailer, C.; Pou, S.; Halpern, H. J.; Robinson, B. H.; Nielsen, R.; Rosen, G. M. *J. Org. Chem.* **2003**, *68*, 7811−7817.
(28) Zhao, H.; Joseph, J.; Zhang, H.; Karoui, H.; Kalyanaraman, B. *Free Radical Biol. Med.* **2001**, *31*, 599−606.
(29) Villamena, F.; Zweier, J. *J. Chem. Soc., Perkin Trans. 2* **2002**, 1340−1344.
(30) Villamena, F. A.; Merle, J. K.; Hadad, C. M.; Zweier, J. L. *J. Phys. Chem. A* **2005**, *109*, 6083−6088.
(31) Labanowski, J. W.; Andzelm, J. *Density Functional Methods in Chemistry*; Springer: New York, 1991.
(32) Parr, R. G.; Yang, W. *Density Functional Theory in Atoms and Molecules*; Oxford University Press: New York, 1989.
(33) Hehre, W. J.; Radom, L.; Schleyer, P. V.; Pople, J. A. *Ab Initio Molecular Orbital Theory*; John Wiley & Sons: New York, 1986.
(34) Becke, A. D. *Phys. Rev. A* **1988**, *38*, 3098.
(35) Becke, A. D. *J. Chem. Phys.* **1993**, *98*, 5648.
(36) Lee, C.; Yang, W.; Parr, R. G. *Phys. Rev. B* **1988**, *37*, 785.
(37) Tomasi, J.; Persico, M. *Chem. Rev.* **1994**, *94*, 2027.
(38) Cossi, M.; Barone, V.; Cammi, R.; Tomasi, J. *Chem. Phys. Lett.* **1996**, *255*, 327.
(39) Barone, V.; Cossi, M.; Tomasi, J. *J. Chem. Phys.* **1997**, *107*, 3210.
(40) Barone, V.; Cossi, M.; Tomasi, J. *J. Comput. Chem.* **1998**, *19*, 404.
(41) Cossi, M.; Barone, V. *J. Chem. Phys.* **1998**, *109*, 6246.
(42) Frisch, M. J.; et al. *Gaussian 98*, revision A.11.3; Gaussian, Inc.: Pittsburgh, PA, 2002.
(43) Frisch, M. J.; et al. *Gaussian 03*, revision B.04; Gaussian, Inc.: Pittsburgh, PA, 2003.
(44) Scott, A. P.; Radom, L. *J. Phys. Chem.* **1996**, *100*, 16502−16513.
(45) *Spartan'04*; Wavefunction, Inc: Irvine, CA, 2004.
(46) Kong, J.; et al. *J. Comput. Chem.* **2000**, *21*, 1532.
(47) Simon, S.; Duran, M.; Dannenberg, J. J. *J. Chem. Phys.* **1996**, *105*, 11024.
(48) Boys, S. F.; Bernardi, F. *Mol. Phys.* **1970**, *19*, 553.
(49) Callam, C. S.; Singer, S. J.; Lowary, T. L.; Hadad, C. M. *J. Am. Chem. Soc.* **2001**, *123*, 11743−11754.
(50) Montgomery, J. A., Jr.; Frisch, M. J.; Ochterski, J. W.; Petersson, G. A. *J. Chem. Phys.* **1999**, *110*, 2822.

(51) Montgomery, J. A., Jr.; Frisch, M. J.; Ochterski, J. W.; Petersson, G. A. *J. Chem. Phys.* **2000**, *112*, 6532.

(52) Barone, V. In *Recent Advances in Density Functional Theory, Part 1*; Cong, D. P., Ed.; World Scientific Publishing Co.: Singapore, 1995; p 287.

(53) Woon, D. E.; Dunning, T. H. *J. Chem. Phys.* **1995**, *103*, 4572.

(54) Adamo, C.; Barone, V. *J. Chem. Phys.* **1999**, *110*, 6158.

(55) Villamena, F.; Rockenbauer, A.; Gallucci, J.; Velayutham, M.; Hadad, C.; Zweier, J. *J. Org. Chem.* **2004**, *69*, 7994−8004.

(56) Rosen, G. M.; Beselman, A.; Tsai, P.; Pou, S.; Mailer, C.; Ichikawa, K.; Robinson, B. H.; Nielsen, R.; Halpern, H. J.; MacKerell, A. D. *J. Org. Chem.* **2004**, *69*, 1321−1330.

(57) Improta, R.; Barone, V. *Chem. Rev.* **2004**, *104*, 1231−1253 and references therein.

(58) Cirujeda, J.; Vidal-Gancedo, J.; Jrgens, O.; Mota, F.; Novoa, J. J.; Rovira, C.; Veciana, J. *J. Am. Chem. Soc.* **2000**, *122*, 11393−11405.

(59) Barone, V.; Bencini, A.; Cossi, M.; Di Matteo, A.; Mattesini, M.; Totti, F. *J. Am. Chem. Soc.* **1998**, *120*, 7069−7078.

(60) Saracino, G. A. A.; Tedeschi, A.; D'Errico, G.; Improta, R.; Franco, L.; Ruzzi, M.; Corvaia, C.; Barone, V. *J. Phys. Chem. A* **2002**, *106*, 10700−10706.

(61) Final optimized structures of the three isomers at the B3LYP/aug-cc-pVDZ level gave final D(N−C−O−O) dihedral angles of $\Theta = 76.3$, 173.0, and 294.0° as conformers A-1, A-2, and A-3, respectively. The predicted hfcc's and spin densities at the B3LYP/aug-cc-pVDZ level are discussed in the Supporting Information. We have also employed various basis sets in the calculation of hfcc's based on published works (see ref 58), for example, EPR-II, EPR-III, cc-pVDZ, and cc-pVTZ based on the B3LYP/aug-cc-pVDZ optimized geometry or B3LYP/6-31G(d) and B1LYP/6-31G(d)//B3LYP/6-31G(d) (see ref 63).

(62) Reed, A. E.; Weinhold, F. A.; Curtiss, L. A. *Chem. Rev.* **1998**, *98*, 899.

(63) Zakrassov, A.; Kaftory, M. *J. Solid State Chem.* **2002**, *169*, 75−80.

(64) Westhof, E.; Sundaralingam, M. *J. Am. Chem. Soc.* **1980**, *102*, 1493.

(65) Sundaralingam, M. *J. Am. Chem. Soc.* **1965**, *87*, 599.

(66) Altona, C.; Sundaralingam, M. *J. Am. Chem. Soc.* **1972**, *94*, 8205.

(67) Harvey, S. C.; Prabhakaran, M. *J. Am. Chem. Soc.* **1986**, *108*, 6128.

(68) Comparison of hfcc's at the B3LYP/6-31+G(d,p) level with the B3LYP/6-31G(d) and PBE0/EPR-II levels for DMPO−OH and DMPO−O_2H shown in the Supporting Information.

(69) For clarity and simplicity, we will only discuss results at the B3LYP/6-31G(d) level, while results at the PBE0/6-31G(d) level are discussed in the Supporting Information.

(70) Eriksson, L. A.; Wang, J.; Boyd, R. J.; Lunell, S. *J. Phys. Chem.* **1994**, *98*, 792−799.

(71) Briere, R.; Rassat, A. *Tetrahedron* **1976**, *32*, 2891−2898.

(72) Villamena, F. A.; Dickman, M. H.; Crist, D. R. *Inorg. Chem.* **1998**, *37*, 1454−1457.

(73) Marriott, P. R.; Perkins, M. J.; Griller, D. *Can. J. Chem.* **1980**, *58*, 803−807.

(74) Tuccio, B.; Lauricella, R.; Frejaville, C.; Bouteiller, J.-C.; Tordo, P. *J. Chem. Soc., Perkin Trans. 2* **1995**, 295−298.

(75) Sankuratri, N.; Kotake, Y.; Janzen, E. G. *Free Radical Biol. Med.* **1996**, *21*, 889−894.

(76) Villamena, F.; Hadad, C. M.; Zweier, J. *J. Am. Chem. Soc.* **2004**, *126*, 1816−1829.

(77) Khramtsov, V. V.; Berliner, L. J.; Clanton, T. L. *Magn. Reson. Med.* **1999**, *42*, 228−234.

(78) Villamena, F. A.; Dickman, M. H.; Crist, D. R. *Inorg. Chem.* **1998**, *37*, 1446−1453.